nature photonics

ARTICLES

https://doi.org/10.1038/s41566-019-0561-9

Higher-order topological states in photonic kagome crystals with long-range interactions

Mengyao Li[1,2], Dmitry Zhirihin[1,3], Maxim Gorlach[3], Xiang Ni[1,2], Dmitry Filonov[4], Alexey Slobozhanyuk[3], Andrea Alù[1,2,5] and Alexander B. Khanikaev[1,2*]

Photonic topological insulators enable topological boundary modes that are resilient to defects and disorder, irrespective of manufacturing precision. This property is known as topological protection. Although originally limited to dimensionality of modes one lower than that of topological insulators, the recently discovered higher-order topological insulators (HOTIs) offer topological protection over an extended range of dimensionalities. Here, we introduce a photonic HOTI with kagome lattice that exhibits topological bulk polarization, leading to the emergence of one-dimensional edge states, as well as higher-order zero-dimensional states confined to the corners of the structure. Interestingly, in addition to the corner states due to nearest-neighbour interactions, we discover a new class of topological corner states induced by long-range interactions and specific to photonic systems. Our findings demonstrate that photonic HOTIs possess richer physics than their condensed-matter counterparts, offering opportunities for engineering novel designer electromagnetic states with unique topological robustness.

Topological systems exhibit unique and often counterintuitive properties, such as robust electronic transport and wave propagation, which promise to revolutionize technologies across a variety of fields, from quantum electronics[1–3] to photonics[4–14] and acoustics[15–17]. In electronics and quantum photonics, topological phenomena have unlocked novel approaches to quantum computing interfaces[18,19] and robust lasing[20–25], while in a broad range of classical fields, including optics, mechanics and acoustics, they offer an unprecedented degree of control and robustness, manifesting as resilience to defects and disorder[5–11,13,16,17,26]. While most topological systems studied so far have been characterized by the presence of topological states with dimensionality one lower than that of the system, recently, a new class of topological systems, the so-called higher-order topological insulators (HOTIs), has been introduced[27–29]. In contrast to conventional topological insulators, HOTIs support topological states[28,30–33] two or more dimensions lower than the system, known as higher-order topological (HOT) states. One example is the distorted graphene-like photonic lattice that was shown to host lower-dimensional localized HOT states[34]. Another example is that of quadrupole topological insulators[27,35], which have been recently implemented in mechanical[36] and photonic[37,38] systems and in electrical circuits[39]. Another class of crystalline insulators with zero Chern number is that of Wannier-type second- and third-order topological insulators, which exhibit topological bulk polarization and support zero-energy states localized at the corners[30,40–43]. Topological corner states in such systems are protected by time reversal and/or spatial symmetries[29,40], which may not only pin them to zero energy and localization at one of the sublattices, but also give rise to their non-radiative character and bound states in their continuum behaviour[41]. It is important to distinguish HOTIs from a broad class of systems where localization of lower-dimensional states can take place on a topological defect[44], for example, induced by a vortex of Kekulé modulation on the lattice, which also can be topologically protected[45]. In contrast to this type of system, in HOTIs, the topological states localize at the external boundaries due to the global property (of the bulk of the material)—topological bulk polarization—and not due to the local change in properties caused by the introduction of the defect (albeit topological).

Here, we design and experimentally demonstrate photonic higher-order corner states in a microwave photonic crystal with topological bulk polarization. In addition to higher-order states consistent with those observed recently in acoustics[41], we show that in electromagnetic systems where far-field interactions among non-neighbouring unit cells are inevitable, the coupling beyond nearest neighbours leads to the emergence of a new class of HOT corner states, which split from the topological edge states continuum. Interestingly, the role of interaction in photonic systems beyond nearest-neighbour coupling has been explored by Leykam et al.[46] in the context of topological photonics to control topological transitions. More relevant to our paper, the effect of next-nearest-neighbour (NNN) coupling on corner and defect states in dimerized Lieb lattices with flat bands has been investigated by Poli et al.[47]. It was shown, both theoretically and in a microwave experiment, that the reduction of the chiral symmetry gives rise to spectrally and isolated robust point-defect zero modes. However, to the best of our knowledge, no emergence of the new type of HOT states have been reported. Our findings, therefore, open up new opportunities for topological photonic metamaterials beyond previously considered approximations based on analogies with electronic systems, and envision devices whose functionality relies on multiplicity of topological states of differing nature and dimensionality interacting with each other in a controllable manner.

Photonic HOTI

We explore a two-dimensional topological photonic crystal[30,48] with topological bulk polarization, supporting a topological phase protected by lattice symmetries. The lattice represents an array of

[1]Department of Electrical Engineering, Grove School of Engineering, City College of New York, New York, NY, USA. [2]Physics Program, Graduate Center of the City University of New York, New York, NY, USA. [3]Department of Nanophotonics and Metamaterials, ITMO University, Saint Petersburg, Russia. [4]Center for Photonics and 2D Materials, Moscow Institute of Physics and Technology, Dolgoprudny, Russia. [5]Photonics Initiative, Advanced Science Research Center, City University of New York, New York, NY, USA. *e-mail: khanikaev@gmail.com

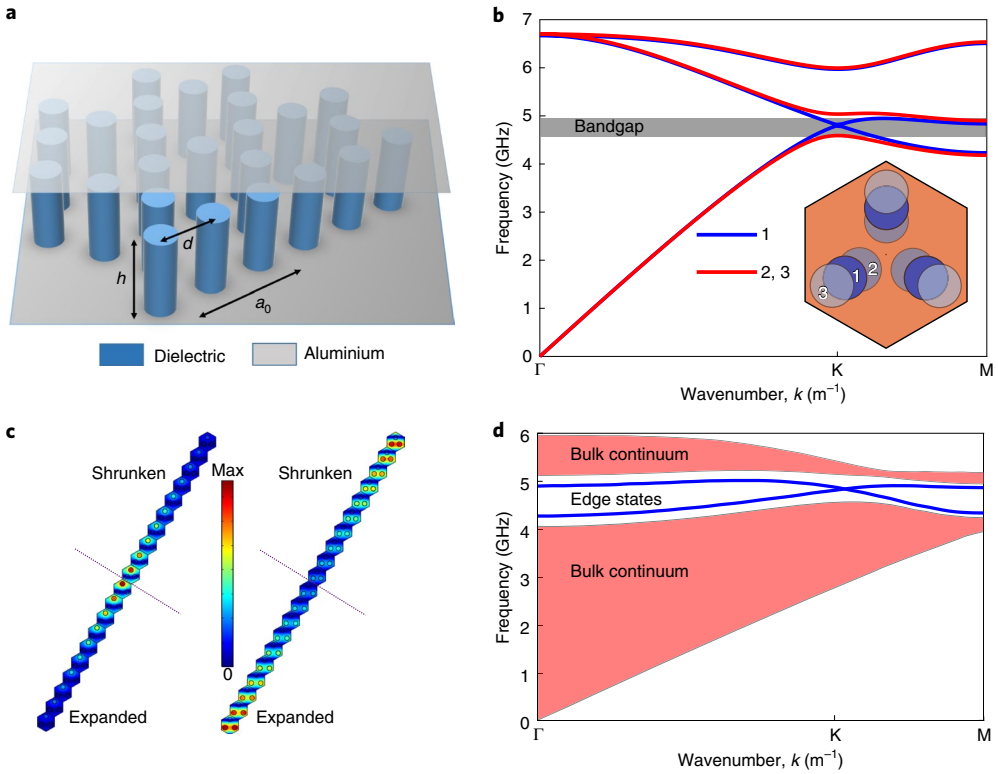

Fig. 1 | Kagome lattice and corresponding bulk and edge band spectra. a, Kagome lattice with dielectric cylinders as sites, with top and bottom bounded by aluminium plates. **b**, Bulk band diagrams of unperturbed (1), shrunken (2) and expanded (3) kagome lattices. A complete bandgap (grey band) is formed in the shrunken and expanded cases due to the symmetry reduction. Inset: corresponding lattice unit cells. **c**,**d**, Simulations of edge states at the boundary between non-trivial (expanded) and trivial (shrunken) lattices, showing field profiles of a kagome supercell structure with shrunken/expanded domain walls, where two modes are localized at the inner and outer interfaces, respectively (**c**), and the corresponding band diagram for the supercell (**d**). h, height of dielectric cylinder; a_0, lattice constant. Γ, K and M are high-symmetry points in the Brillouin zone of a kagome lattice. The colour scale in **c** shows the amplitude of the electric field (V m^{-1}).

dielectric cylinders arranged to form a kagome lattice between two parallel aluminium plates, as shown in Fig. 1a. Dielectric cylinders are formed by filling the patterned Styrofoam mould with a high-index dielectric material. In this geometry, the dielectric cylinders support a vertical dipolar mode that is also the lowest-frequency mode we choose to work with to design the topological photonic crystal. In addition to the near-field coupling of the dipolar modes in the lattice, the modes also couple to the transverse electromagnetic mode supported by the parallel-plate host waveguide formed by aluminium plates, thus giving rise to far-field radiative coupling. The latter coupling renders previous analytical treatments of topological kagome lattices inadequate for the photonic system at hand, as we need to consider interactions beyond nearest-neighbour approximations (Supplementary Section C) and apply first-principles methods to rigorously analyse the system. Nonetheless, the coupling strength between cylinders can still be tuned by shifting the cylinders closer to or farther away from one another, thus enabling control over the coupling within the lattice. By comparing the analytical tight-binding model and first-principles simulations (using the finite-element method (FEM) software COMSOL Multiphysics and the radio frequency module), we find that the system is qualitatively well described by the tight-binding model when NNN coupling is considered (Supplementary Sections A and C).

For the case of an ideal (unperturbed) kagome lattice, for which the distances between cylinders, d, in the same and nearby unit cells are equal (Fig. 1b inset, position 1), that is, the inter-cell and intra-cell couplings are the same, the band diagram with FEM simulations (blue lines in Fig. 1b) exhibits a Dirac-like degeneracy at the K (and K′) point in the Brillouin zone. When the crystalline symmetry is reduced by shifting the dielectric cylinders as shown in the Fig. 1b inset (positions 2 and 3), the inter-cell and intra-cell couplings between neighbouring trimers are no longer equal. This induces a topological transition and leads to the opening up of a complete photonic bandgap at the K and K′ points.

The topologically non-trivial expanded structure (position 3) and trivial shrunken structure (position 2) have identical band structures, shown in Fig. 1b by red lines. Therefore, the two cases cannot be distinguished by frequency dispersion alone. However, these two configurations exhibit two distinct topological phases, separated by the gapless (position 1) transition point corresponding to the ideal kagome lattice. The topological transition arises due to the symmetry reduction caused by the 'trimerization' of the lattice, giving rise to the hybridization and band inversion of formerly degenerate bands. The topological transition can be demonstrated directly by calculating the topological bulk polarization through a Wilson loop, and by investigating the C_3 symmetry-related properties at high-symmetry points in the Brillouin zone, as discussed in Supplementary Section AII.

The topological bulk polarization characterizes the displacement of the average position of the Wannier centre from the centre of the unit cell[28,35]. In the trivial case, the zero value of bulk polarization implies that the Wannier centre is pinned to the centre of the unit cell, and no modes can dangle at the boundaries. However, in the topological non-trivial case, the non-vanishing bulk polarization induces a shift of the Wannier centre, so that when the boundaries are introduced, dangling states emerge at the boundaries[41].

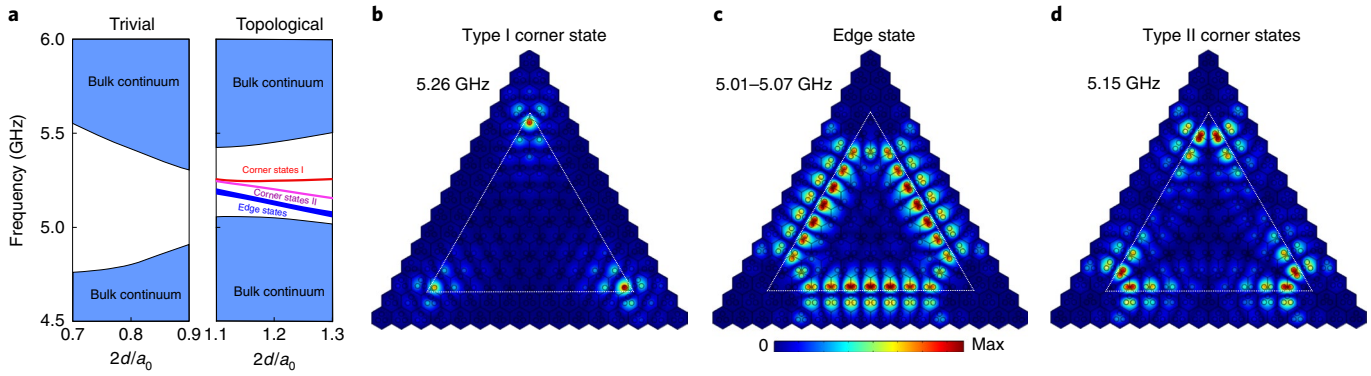

Fig. 2 | Simulation results of topological edge states and type I and type II corner states. a, Energy spectrum for the triangular kagome lattice with $\kappa = 2d/a_0$ in trivial ($\kappa < 1$) and topological ($\kappa > 1$) regimes. **b**–**d**, Field profiles and their corresponding frequencies. Both corner states (type I (**b**), red band in **a**, and type II (**d**), magenta band in **a**) and edge states (**c**) (blue band in **a**) appear in the bandgap of the topological region and are gapped from each other. Both type I and II corner states are triply degenerate states. Colour bar in **b**–**d** shows the amplitude of the electric field (V m^{-1}).

The bulk polarization difference of the expanded kagome lattice acquires values (1/3, 1/3) relative to the shrunken lattice. We have also proven that with the inclusion of long-range interactions, the bulk polarization remains quantized and equals (1/3, 1/3), leading to the emergence of boundary states in finite crystals surrounded by trivial domains. Details of the calculations of the topological polarization and the Wannier centre (both for systems with and without long-range interactions) are outlined in Supplementary Section AII.

Given the bulk–boundary correspondence for our system[41], the non-trivial polarization difference across domains manifests in the emergence of topological edge states, which appear at the domain walls separating shrunken and expanded domains of the crystal. These states can be clearly seen in the eigenfrequency simulations of a supercell of 20 unit cells with domain walls in the centre and at the outer edges (the latter due to periodic boundary conditions imposed at the outer vertical boundaries). The field profiles in Fig. 1c show two modes localized at the inner and outer interfaces, respectively, and the corresponding bands are clearly visible in the band diagram, Fig. 1d (blue lines), within the topological bandgap separating the bulk continuum (red shaded regions).

More interestingly, the distorted kagome lattice is expected to exhibit HOT states for the case of the finite structure. These states represent second-order topological states confined to zero-dimensional corners of our two-dimensional system when the angle of the corner is 60°. As has been previously demonstrated[41], in the case when only nearest-neighbour coupling is present, these HOT states seem to be pinned to a single frequency, which exactly equals the resonance frequency of a single isolated resonator in the lattice and is referred to as zero energy. These states seem to be protected by the generalized chiral symmetry, which guarantees that the corner states are pinned to zero energy, and are ideally localized at one of the sublattices. The generalized chiral symmetry for the present case of a two-dimensional kagome lattice is described by the operator $\hat{\Gamma}_3$, with the property $\hat{\Gamma}_3^3 = 1$, connecting a sequence of inequivalent Hamiltonians $\hat{H}_n$ with the same spectrum $\hat{\Gamma}^n \hat{H}_0 \hat{\Gamma}^{-n} = \hat{H}_n$, where $n = 1, 2$, and $\hat{H}_0$ is the original Hamiltonian of the system, so that $\hat{H}_0 + \hat{H}_1 + \hat{H}_2 = 0$. Importantly, in the context of electromagnetic systems, when long-range interactions are inevitable, our analysis shows that the generalized chiral symmetry is retained as long as interactions within the same sublattice are negligible (for details, see Supplementary Section A).

The results of first-principles simulations for the distorted crystal of triangular shape bounded by a trivial (shrunken) domain in Fig. 2a show the evolution of the band structure as the system undergoes a topological transition when the ratio of inter- to intra-cell distance (from shrunken to expanded) is gradually detuned. As expected from the above discussion, the topological states appear only in the non-trivial case of the expanded lattice, characterized by non-vanishing bulk polarization. In Fig. 2b, we can indeed see the corner states, which we refer to as type I HOT states and do localize on a particular sublattice within the topological domain[41], indicating the presence of the generalized chiral symmetry. The triply degenerate and flat spectral position of type I corner states for all three corners (Fig. 2a) confirms that third-order and longer-range interactions within the same sublattice, which break the generalized chiral symmetry, are very weak. We attribute this to the screening of such interactions by the rods of two other sublattices located exactly between the rods of the same sublattice.

HOT states induced by long-range interactions

Besides type I corner modes, another interesting observation can be made for the case of a finite domain by inspecting Fig. 2a and the corresponding eigenmode field profiles of Fig. 2d. Three (degenerate) modes follow closely the spectrum of the topological edge states as the coupling detuning parameter $\kappa = 2d/a_0$ increases within the topological regime. For values of $\kappa \approx 1.1$, the corresponding eigenmodes have a field profile similar to that of edge states, but they tend to localize to corners as κ increases in value, establishing an interesting new type of HOT corner states, which we refer to as type II. Interestingly, the tight-binding model that considers only nearest-neighbour coupling fails to predict these states, thus suggesting that their nature is specific to systems with long-range interactions, that is, these new states can be linked to the electromagnetic interactions beyond nearest-neighbouring cylinders. Indeed, the tight-binding model simulations with NNN interactions reveal these new type II corner modes, which, just as in the case of first-principles electromagnetic studies, split off from the edge states continuum (Fig. 3b,d,e and Supplementary Section AI) and have field profiles resembling those of the topological edge states, but exponentially decaying away from the corners. This observation allows us to draw the conclusion that type II HOT corner states form due to the localization of the topological edge states at the corners, which is caused by long-range interactions (more details are available in Supplementary Section AI).

To better understand the origin of type II HOT states, we developed the perturbation theory, starting from the limiting case of a fully 'trimerized' (in analogy with the fully dimerized limit of the one-dimensional Su–Schrieffer–Heeger model) topological lattice with intra-cell coupling $K = 0$ and NNN hopping $J_2 = 0$. In this case, an entire structure splits into isolated clusters of sites connected to each other via only inter-cell coupling J, as illustrated in Fig. 3a. Thus, the bulk of the lattice consists of trimers, which support two

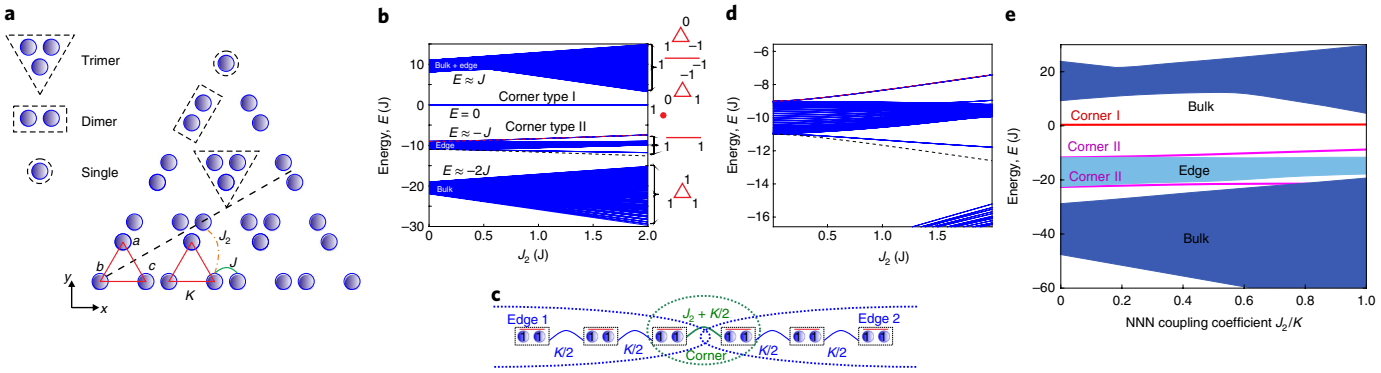

Fig. 3 | Localization mechanism of type II corner states. a, Finite triangle-shaped geometry of the kagome lattice. Red triangles show boundaries of the unit cell; the diagonal black dashed line is the bisectrix of the corner. Inset: isolated sets of interacting sites: trimers in the bulk, dimers at the edges and single isolated sites at the corners. **b**, Energy spectrum and eigenmodes of a finite lattice (630 sites) for $J/K=10$, and with varying ratio J_2/K *(assuming* $K=1$ J). **c**, Illustration of coupling between dimers at a corner forming type II corner states. **d**, Enlarged section of **b** showing the bands of edge states and the emergence of type II HOT states as J_2 increases. Red (for antisymmetric mode) and black (for symmetric mode) dashed lines show the analytical result for the energies of corner states obtained with first-order perturbation theory. **e**, Result of tight-binding model for the same structure as in **b** but far from the limit of the trimerized lattice ($K=5$ J, $J/K=3.5$).

types of mode: (1) a singlet monopolar mode with equal amplitudes at all three sites and energy $E=-2J$ (Fig. 3b) and (2) a doublet of dipolar modes with energy equal to J. Once we assume some small but non-zero values of K or J_2, these discrete modes give rise to the formation of dispersive bulk bands, depicted in Fig. 3b.

Conversely, the edges of the structure consist of isolated (dangling) dimers, which support symmetric and antisymmetric modes with energies $-J$ and J, respectively. Note that the former set of modes gives rise to the topological edge states of the lattice, while the latter set overlaps and merges with the continuum of upper (dipolar) bulk bands.

Finally, the corners of the structure in Fig. 2a represent isolated sites, a consequence of which is the triply degenerate corner modes with the energies of isolated sites. As mentioned above, these modes represent type I HOT states protected by the generalized chiral symmetry, which ensures that their energy remains pinned to zero-energy level, even when both J_2 and K take non-zero values (see detailed symmetry analysis in Supplementary Section A). As this type of zero-energy corner mode appears even in the absence of NNN coupling, we do not explore it any further.

Since in the limiting case of the trimerized lattice ($J_2=K=0$), the eigenmodes of the lattice can be written down analytically, as we show in Supplementary Section C, we can immediately apply the degenerate perturbation theory to reveal the role of the NNN coupling in the formation of the type II HOT corner modes and to deduce the energy and localization length of these modes.

The result of the first-order perturbation theory is schematically shown in Fig. 3c, which illustrates that the boundary problem reduces to the effective one-dimensional problem, with two edges (blue sectors) meeting at the corner (green sector). The analysis shows that the interaction among (symmetric) modes of the individual dimers along the edges, which equals $K/2$, seems to be weaker than the interaction between the proximal dimers across the corner by the strength of J_2. Straightforward calculations yield two localized solutions with

$$E = -J \mp \frac{(K+2J_2)^2+K^2}{2K+4J_2} \qquad (1)$$

where upper and lower signs ($\mp$) correspond to two type II HOT states, which are symmetric and antisymmetric, respectively, with respect to reflection relative to the bisectrix of the corner. The calculations also demonstrate that these states decay exponentially away from the corner.

For comparison, the energies of symmetric and antisymmetric corner modes calculated using such reduction to the effective one-dimensional problem are plotted by the black and red dashed lines, respectively, in Fig. 3d, along with the exact solution to the tight-binding problem (blue lines). It is seen that the lower-energy (symmetric) type II mode strongly interacts with the continuum of the lower-energy bulk states, and for larger K and J_2 values, it strongly hybridizes with the continuum. At the same time, an antisymmetric corner mode always appears within the bandgap and nicely follows the analytic solution of the perturbation theory. Considering more realistic regimes far from the fully trimerized lattice (Fig. 3e), the results perfectly agree with our conclusions and explain why the (symmetric) lower-energy mode is not observed in the first-principles FEM simulations. Indeed, for our case of a less trimerized photonic lattice with stronger NNN coupling, this mode is pushed into the lower bulk continuum and is destroyed through mixing with the bulk states.

Experimental results

To experimentally validate our theoretical predictions, we have fabricated crystal with ten unit cells per triangle side length, placed in a parallel-plate waveguide, and performed near-field measurements. Figure 4a presents the extracted local density of states, which were retrieved from the measured field profiles by applying different spatial filter functions that take into account the field profiles of the respective modes. For type I corner states (Fig. 4b), the spatial filter is the Heaviside step function placed over the three corner cylinders. For type II corner states (Fig. 4c), the filter is the step function over pairs of cylinders adjacent to the corner site. For the topological edge states (Fig. 4d), all edge cylinders except those at and adjacent to the corner are included in the spatial filter, while for bulk states, all internal cylinders are considered. The extracted experimental densities of states are in excellent agreement with the results of theoretical calculations as they all peak at the respective frequencies of the type I and II corner states and overlap spectrally with the edge band. The field profiles corresponding to the frequencies of the maximal density of corner states are also consistent with the theoretical results in Fig. 2c,d. In particular, for type I states, both theoretical and experimental results clearly reveal localization of the field to the sublattice of upper cylinders in the topological

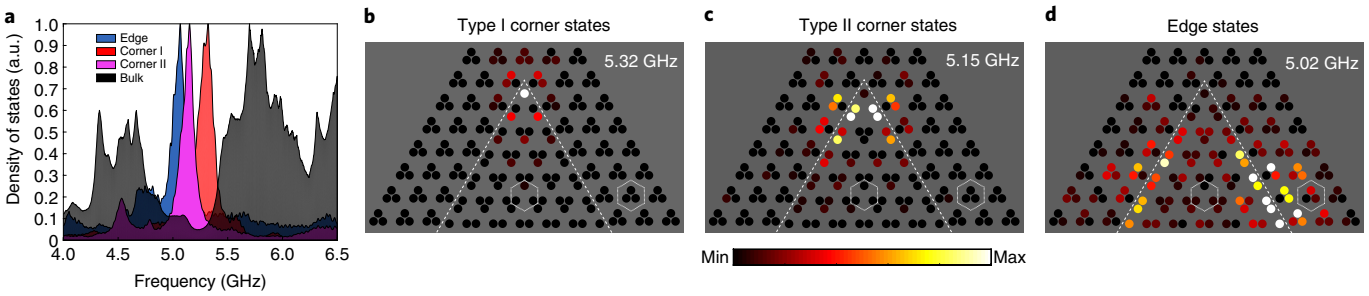

Fig. 4 | Experimental observation of HOT type I and type II corner and edge states. a, Experimentally measured densities of states. Coloured areas are experimental results for corner excitation, and black areas are for bulk excitation. **b**–**d**, Field profiles (log scaled electric field intensity (V m^{-1})) showing different types of topological corner states (type I (**b**) and type II (**c**)) and edge state (**d**), observed experimentally at corresponding frequencies when the system is excited by a source placed at near the corner. a.u., arbitrary units. In **b**–**d**, the white dashed lines show the boundary between expanded triangle and shrunken crystal around it, and the white hexagons show the unit cells of the crystals.

region, indicating the presence of the generalized chiral symmetry. Moreover, the interactions beyond nearest neighbours clearly give rise to the emergence of a new, type II, HOT state, with a field profile (Fig. 3c) that confirms its origin from the edge continuum, localized due to such interactions.

To ensure the generality of our findings in the context of electromagnetics, we examined two additional cases of boundary conditions specific to electromagnetic problems. In the first case, we studied an open topological crystal bounded by empty space (unfilled parallel-plate waveguide). This type of boundary enables coupling between modes of the crystal and the waveguide and is known to give rise to radiative losses and finite lifetime of the modes, the subject of interest in the context of non-Hermitian topological phases[49,50]. We found that for our system, the leakage did not bring any new physics besides spectral broadening of the HOT and topological edge states, thus evidencing their robustness with respect to the open boundary condition. The second boundary condition studied was the case of a topological domain surrounded by a metal wall. In this case, the experimental studies confirmed the presence of both types of HOT state, as well as topological edge states, but the chiral symmetry was clearly broken, leading to spectral shift of the modes. A detailed description of both experiments is provided in Supplementary Section B.

Summary

In this work, we have demonstrated that the physics of HOT states in photonic structures can be distinct from their condensed-matter and acoustic counterparts, despite a similar geometry and topological phase. In particular, the presence of near- and far-field interactions in electromagnetic systems provides richer opportunities by enabling topological states not immediately available in electronic systems. In the photonic kagome crystal considered here, we discovered type I HOT corner states protected by the generalized chiral symmetry. More importantly, we found theoretically, and confirmed experimentally, that long-range interactions can result in the formation of a new class of type II HOT corner states. Our studies also reveal an inherent robustness of corner states to different boundary conditions, making photonic HOTIs suitable for integration into different device platforms. In particular, we have experimentally confirmed that the HOT corner states persist when the crystal is bounded by topologically trivial crystal, is surrounded by free space or is terminated by a conductor. The first two cases clearly show that the proposed designs can be immediately realized in optical domains where metals are lossy.

Our study demonstrates the major potential of photonic HOTIs for revealing new fundamental phenomena stemming from physics that are specific to electromagnetic systems. It also shows that photonic HOTIs represent an exceptional platform for the realization of tuneable and robust devices with highly controllable field localization and spectral characteristics across the entire electromagnetic spectrum. The peculiar interplay between long-range interactions and topology has been shown to lead to the transformation of edge states into a new class of HOT corner states, which enables coupling topological states of differing dimensionalities. Extending our ideas to higher-dimensional photonic systems, as well as to synthetic dimensions, opens up even broader opportunities for novel photonic HOTIs. Originating from lower-order topological states due to their localization induced by long-range interactions, such states can be tailored on demand to design and construct a variety of interfaces and platforms of interacting topological states of different orders.

Online content

Any methods, additional references, Nature Research reporting summaries, source data, extended data, supplementary information, acknowledgements, peer review information; details of author contributions and competing interests; and statements of data and code availability are available at https://doi.org/10.1038/s41566-019-0561-9.

Received: 28 March 2019; Accepted: 30 October 2019;
Published online: 9 December 2019

References

1. Hasan, M. Z. & Kane, C. L. Colloquium: topological insulators. *Rev. Mod. Phys.* **82**, 3045–3067 (2010).
2. Qi, X. L. & Zhang, S. C. Topological insulators and superconductors. *Rev. Mod. Phys.* **83**, 1057–1110 (2011).
3. Bernevig, B. A. & Hughes, T. L. *Topological Insulators and Topological Superconductors* (Princeton University Press, 2013).
4. Raghu, S. & Haldane, F. D. M. Analogs of quantum-Hall-effect edge states in photonic crystals. *Phys. Rev. A* **78**, 033834 (2008).
5. Wang, Z., Chong, Y., Joannopoulos, J. D. & Soljacic, M. Observation of unidirectional backscattering-immune topological electromagnetic states. *Nature* **461**, 772–775 (2009).
6. Hafezi, M., Demler, E. A., Lukin, M. D. & Taylor, J. M. Robust optical delay lines with topological protection. *Nat. Phys.* **7**, 907–912 (2011).
7. Fang, K., Yu, Z. & Fan, S. Realizing effective magnetic field for photons by controlling the phase of dynamic modulation. *Nat. Photon.* **6**, 782–787 (2012).
8. Fang, K. & Fan, S. Controlling the flow of light using the inhomogeneous effective gauge field that emerges from dynamic modulation. *Phys. Rev. Lett.* **111**, 203901 (2013).
9. Khanikaev, A. B. et al. Photonic topological insulators. *Nat. Mater.* **12**, 233–239 (2013).
10. Rechtsman, M. C. et al. Photonic Floquet topological insulators. *Nature* **496**, 196–200 (2013).
11. Plotnik, Y. et al. Observation of unconventional edge states in 'photonic graphene'. *Nat. Mater.* **13**, 57–62 (2014).

12. Wu, L. H. & Hu, X. Scheme for achieving a topological photonic crystal by using dielectric material. *Phys. Rev. Lett.* **114**, 223901 (2015).
13. Cheng, X. et al. Robust reconfigurable electromagnetic pathways within a photonic topological insulator. *Nat. Mater.* **15**, 542–548 (2016).
14. Ozawa, T. et al. Topological photonics. *Rev. Mod. Phys.* **91**, 015006 (2019).
15. Xiao, M. et al. Geometric phase and band inversion in periodic acoustic systems. *Nat. Phys.* **11**, 240–244 (2015).
16. Yang, Z. et al. Topological acoustics. *Phys. Rev. Lett.* **114**, 114301 (2015).
17. Huber, S. D. Topological mechanics. *Nat. Phys.* **12**, 621–623 (2016).
18. Barik, S. et al. A topological quantum optics interface. *Science* **359**, 666–668 (2018).
19. Kitaev, A. Unpaired Majorana fermions in quantum wires. *Phys.-Usp.* **44**, 131–136 (2001).
20. Bahari, B. et al. Nonreciprocal lasing in topological cavities of arbitrary geometries. *Science* **358**, 636–639 (2017).
21. Bandres, M. A. et al. Topological insulator laser: experiments. *Science* **359**, eaar4005 (2018).
22. Harari, G. et al. Topological insulator laser: theory. *Science* **359**, eaar4003 (2018).
23. St-Jean, P. et al. Lasing in topological edge states of a one-dimensional lattice. *Nat. Photon.* **11**, 651–656 (2017).
24. Zhao, H. et al. Topological hybrid silicon microlasers. *Nat. Commun.* **9**, 981 (2018).
25. Parto, M. et al. Edge-mode lasing in 1D topological active arrays. *Phys. Rev. Lett.* **120**, 113901 (2018).
26. Ni, X. et al. Spin- and valley-polarized one-way Klein tunneling in photonic topological insulators. *Sci. Adv.* **4**, eaap8802 (2018).
27. Benalcazar, W. A., Bernevig, B. A. & Hughes, T. L. Quantized electric multipole insulators. *Science* **357**, 61–66 (2017).
28. Song, Z., Fang, Z. & Fang, C. $(d-2)$-dimensional edge states of rotation symmetry protected 437 topological states. *Phys. Rev. Lett.* **119**, 246402 (2017).
29. Schindler, F. et al. Higher-order topological insulators. *Sci. Adv.* **4**, eaat0346 (2018).
30. Ezawa, M. Higher-order topological insulators and semimetals on the breathing kagome and pyrochlore lattices. *Phys. Rev. Lett.* **120**, 026801 (2018).
31. Geier, M., Trifunovic, L., Hoskam, M. & Brouwer, P. W. Second-order topological insulators and superconductors with an order-two crystalline symmetry. *Phys. Rev. B* **97**, 205135 (2018).
32. Khalaf, E. Higher-order topological insulators and superconductors protected by inversion symmetry. *Phys. Rev. B* **97**, 205136 (2018).
33. Liu, T., He, J. J. & Nori, F. Majorana corner states in a two-dimensional magnetic topological insulator on a high-temperature superconductor. *Phys. Rev. B* **98**, 245413 (2018).
34. Noh, J. et al. Topological protection of photonic mid-gap defect modes. *Nat. Photon.* **12**, 408–415 (2018).
35. Benalcazar, W. A., Bernevig, B. A. & Hughes, T. L. Electric multipole moments, topological multipole moment pumping, and chiral hinge states in crystalline insulators. *Phys. Rev. B* **96**, 245115 (2017).
36. Serra-Garcia, M. et al. Observation of a phononic quadrupole topological insulator. *Nature* **555**, 342–345 (2018).
37. Peterson, C. W., Benalcazar, W. A., Hughes, T. L. & Bahl, G. A quantized microwave quadrupole insulator with topologically protected corner states. *Nature* **555**, 346–350 (2018).
38. Mittal, S. et al. Photonic quadrupole topological phases. *Nat. Photon.* **13**, 692–696 (2019).
39. Imhof, S. et al. Topolectrical-circuit realization of topological corner modes. *Nat. Phys.* **14**, 925–929 (2018).
40. Benalcazar, W. A., Li, T. & Hughes, T. L. Quantization of fractional corner charge in C_n-symmetric topological crystalline insulators. *Phys. Rev. B* **99**, 245151 (2019).
41. Ni, X., Weiner, M., Alù, A. & Khanikaev, A. B. Observation of higher-order topological acoustic states protected by generalized chiral symmetry. *Nat. Mater.* **18**, 113–120 (2019).
42. Weiner, M., Ni, X., Li, M., Alu, A. & Khanikaev, A. B. Demonstration of a 3rd order hierarchy of topological states in a three-dimensional acoustic metamaterial. Preprint at https://arxiv.org/abs/1903.00428 (2019).
43. El Hassan, A. et al. Corner states of light in photonic waveguides. *Nat. Photon.* **13**, 697–700 (2019).
44. Teo, J. C. Y. & Kane, C. L. Topological defects and gapless modes in insulators and superconductors. *Phys. Rev. B* **82**, 115120 (2010).
45. Seradjeh, B., Weeks, C. & Franz, M. Fractionalization in a square-lattice model with time-reversal symmetry. *Phys. Rev. B* **77**, 033104 (2008).
46. Leykam, D., Mittal, S., Hafezi, M. & Chong, Y. Reconfigurable topological phases in next-nearest-neighbor coupled resonator lattices. *Phys. Rev. Lett.* **121**, 023901 (2018).
47. Poli, C., Schomerus, H., Bellec, M., Kuhl, U. & Mortessagne, F. Partial chiral symmetry-breaking as a route to spectrally isolated topological defect states in two-dimensional artificial materials. *2D Mater.* **4**, 025008 (2017).
48. Ni, X., Gorlach, M. A., Alu, A. & Khanikaev, A. B. Topological edge states in acoustic kagome lattices. *New J. Phys.* **19**, 055002 (2017).
49. Bliokh, K. Y., Leykam, D., Lein, M. & Nori, F. Topological non-Hermitian origin of surface Maxwell waves. *Nat. Commun.* **10**, 580 (2019).
50. Liu, T. et al. Second-order topological phases in non-Hermitian systems. *Phys. Rev. Lett.* **122**, 076801 (2019).

Methods

Device fabrication. The crystal was realized in a Styrofoam triangular substrate (relative permittivity around 1.1 and negligible losses) with machine-drilled holes filled by a commercially available dielectric (ceramic aluminium oxide ECCOSTOCK HiK, Emerson & Cuming, with relative permittivity $\varepsilon_r = 10$ and loss tangent $\tan\delta = 0.0007$ as specified in the product datasheet). The geometric dimensions of the structure are as follows: the length and diameter of the cylinders are 20 mm and 6 mm, respectively, and the lattice constant is 24 mm. The shrunken/expanded structure had the distance between cylinders reduced/increased by 30%. The fabricated metacrystal was wrapped with conducting (aluminium) foil, and the modes were excited at the corner by placing a dipole antenna into the hole drilled in the lower metal plate. The field probing was done by another dipole antenna placed into another hole drilled in the upper metal plate, with both plate and antenna moving together across the structure to map the field distribution.

Data availability

Data that are not already included in the paper and/or in the Supplementary Information are available on request from the authors.

Acknowledgements

This work was supported by the Defense Advanced Research Projects Agency under the Nascent programme with grant no. HR00111820040 and by the National Science Foundation with grant nos EFRI-1641069 and DMR-1809915. Experimental investigation of corner states was partially supported by the Russian Science Foundation (grant no. 16-19-10538). Theoretical analysis of type II corner states was partially supported by the Russian Foundation for Basic Research (grant no. 18-32-20065).

Author contributions

A.B.K. initiated the research. M.L., X.N. and M.G. derived the theoretical results. M.L. and D.Z. performed numerical simulations and designed the structure. D.Z., D.F. and A.S. designed and carried out the experiment. M.L. and D.Z. performed the data analysis. A.B.K. and A.A. supervised the research and wrote the main text. All authors discussed the results and contributed to the final version of the manuscript.

Competing interests

The authors declare no competing interests.

Additional information

Supplementary information is available for this paper at https://doi.org/10.1038/s41566-019-0561-9.

Correspondence and requests for materials should be addressed to A.B.K.

Reprints and permissions information is available at www.nature.com/reprints.